Geochemical Perspectives Letters

MnO/MgO ratios of arc basalts highlight the role of early garnet fractionation

B.Z. Klein[1*], O. Müntener[1]

OPEN ACCESS

https://doi.org/10.7185/geochemlet.2309

Abstract

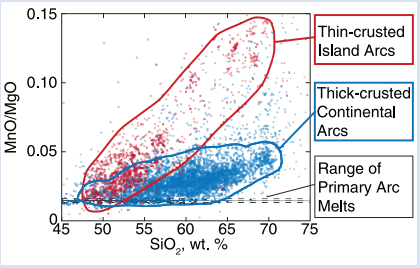

Multiple lines of evidence suggest that garnet may play an important role in the generation of arc magmas, either as a residual phase during mantle melting or subsequently during crystallisation differentiation. Moreover, garnet stability is strongly pressure sensitive, and therefore garnet fractionation can serve as an indirect indicator of fractionation pressure. Here, we introduce MnO/MgO ratios as a compositional proxy uniquely sensitive to garnet fractionation. We show that primary mantle melts have nearly invariant MnO/MgO ratios that are in equilibrium with mantle olivine. Therefore, the subsequent evolution of this ratio is only a function of magmatic differentiation. Further, based on compiled experimental studies, garnet is the only phase that crystallises from basaltic magmas and preferentially partitions MnO relative to MgO. Thus, limited increases in MnO/MgO ratios during magmatic differentiation, as we observe in most continental arcs, are strong evidence for early garnet fractionation and require that crystallisation differentiation begins at or below the Moho of many arcs.

Received 18 November 2022 | Accepted 9 February 2023 | Published 16 March 2023

Introduction

The fractionation of garnet from subduction zone magmas is hypothesised to play a critical role in several fundamental arc processes: delamination of garnet-rich, density unstable cumulates may be critical to the production and stabilisation of continental crust (Jagoutz and Behn, 2013), while fractionation of ferrous iron-rich garnet may contribute to the generation of oxidised, calc-alkaline arc magmas (Tang *et al.*, 2018). These hypotheses are supported by observations from exhumed arc lower crustal sections and xenoliths, which commonly include garnet-rich lithologies (Ducea and Saleeby, 1996; Jagoutz, 2010), and by experimental studies that show that garnet is a stable phase in hydrous magmas at typical arc lower crustal conditions (Alonso-Perez *et al.*, 2009; Ulmer *et al.*, 2018). However, primary garnet phenocrysts are rare in typical arc lavas, making the ubiquity of garnet fractionation at modern arcs difficult to assess.

As an alternative approach, many researchers have highlighted the distinctive heavy rare earth element (HREE)-enriched trace element signature of garnet and argued that garnet must play an important role in the petrogenesis of evolved magmas with complementary HREE depletions. Early applications of this approach focused on Archean tonalite-trondhjemite-granodiorite suites (TTGs) and modern dacites with elevated Sr/Y and La/Yb ratios and argued that these magmas represent partial melts of garnet-bearing subducted crust (Drummond and Defant, 1990). More recently, trace element ratios including Sr/Y, Dy/Yb, and La/Yb were proposed as proxies for crustal thickness (Chapman *et al.*, 2015; Profeta *et al.*, 2015), based on the interpretation that they reflect increased extents of differentiation at pressures high enough to stabilise garnet (*e.g.*, Davidson *et al.*, 2007).

These two approaches use the same trace element ratios to infer distinct processes at different locations within subduction zone systems. Therefore, in the absence of additional observations, interpretations of these ratios alone are necessarily non-unique. In this paper, we introduce melt MnO/MgO ratios as an alternative indicator of garnet fractionation based on two findings: primary mantle melts have comparatively uniform MnO/MgO ratios; and the Mn-Mg partition coefficient between garnet (gt) and melt, defined as $K_D^{Mn\text{-}Mg} = (Mn_{gt}/Mn_{melt})/(Mg_{gt}/Mg_{melt})$, is greater than 1, unique among typical early fractionating phases.

Variability of Subduction Zone Primary Melts

Proxies for garnet differentiation and crustal thickness using trace element ratios, including Sr/Y and La/Yb, have been developed primarily for application to relatively evolved lavas. The rationale for these proxies is that fractionation of garnet-rich cumulates or, equivalently, extraction of partial melts from garnet-rich residues, causes depletions in HREEs, resulting in differentiated melts with elevated trace element ratios. While garnet fractionation may generate this signal, inferring this process based on only the values of these ratios in differentiated magmas requires independent knowledge of the derivative magma's parental melt composition. Without this information, it is not possible to attribute elevated trace element ratios in differentiated magmas to garnet fractionation rather than to inherited parental magma compositions.

1. Institute of Earth Sciences, University of Lausanne, Switzerland
* Corresponding author (email: benjaminzachary.klein@unil.ch)

A recent compilation of primary arc lava compositions (Schmidt and Jagoutz, 2017) highlights this problem. These samples have compositions in equilibrium with typical mantle peridotite, and thus have necessarily undergone minimal differentiation within the crust. However, these lavas display a wide range in both Sr/Y and La/Yb ratios that show no correlation with crustal thickness (Fig. 1). In contrast, both ratios are strongly correlated with primary melt type, regardless of crustal thickness or upper plate type: tholeiitic magmas have uniformly low Sr/Y and La/Yb ratios, while calc-alkaline magmas span a wide range. This large range in primary arc magma incompatible trace element ratios reflects several factors, including variable contributions from the slab (*e.g.*, Elliott, 2004) and degree of prior mantle depletion (*e.g.*, Kelley *et al.*, 2006).

During differentiation, a range of processes beyond garnet fractionation can further modify these ratios. Plagioclase accumulation generates magmas with elevated Sr and Sr/Y ratios (Vukadinovic, 1993), while amphibole fractionation can produce magmas with elevated La/Yb ratios (Davidson *et al.*, 2007). These additional processes are much less sensitive to pressure compared to garnet fractionation, and instead are dominantly sensitive to magmatic H_2O contents. Given the range of primary melt compositions and these additional confounding processes, it is unlikely that the trace element ratios of any single suite of differentiated arc magmas provide meaningful estimates of crustal thickness.

MnO/MgO Ratios in Primary Arc Melts

In contrast to incompatible trace element ratios, the behaviour of most compatible elements in mantle melts is controlled by melting reactions in the mantle wedge. Typically, these elements and their ratios vary predictably in response to changes in mantle melting regime (*e.g.*, Grove *et al.*, 2013), while some canonical ratios, such as Mg# (molar Mg/(Mg + Fe)), display a relatively invariant range reflective of equilibrium with mantle olivine. In Figure 2a, we show that the MnO/MgO ratios of primary arc magmas are also tightly clustered and, based on a recent model of olivine-melt Mn/Mg partitioning (Blundy *et al.*, 2020), are consistent with control by equilibration with mantle olivine (Fig. 2b). These primary melt compositions are inconsistent with garnet-present mantle melting, as this process produces melts with distinctively low MnO/MgO ratios (≤0.01; Walter, 1998). This is consistent with observations that most garnet is exhausted at moderate extents of melting at typical sub-arc mantle conditions (≤11 wt. % melt at 3 GPa; Kushiro, 1996), and with final mantle equilibration at pressures lower than the spinel-garnet transition (Perrin *et al.*, 2016).

These primary lavas show a wide range of incompatible trace element ratios indicative of variable slab contributions (Fig. 1). However, their MnO/MgO ratios are uncorrelated with these trace element ratios (Fig. S-1) and show negligible evidence for control by slab contributions: subducted sediments have elevated MnO/MgO ratios compared to the sub-arc mantle (Plank, 2014), and this elevated ratio is inherited by slab-derived melts or fluids despite equilibrating with garnet-rich residue (Schmidt *et al.*, 2004). The apparent contradiction between incompatible trace element ratios and the MnO/MgO ratios is resolved with a simple mass balance argument: unlike incompatible trace elements, slab derived fluids and melts typically contain an order of magnitude less MnO and MgO than the final melt in equilibrium with the mantle, and thus can exert only minimal control on the eventual MnO/MgO ratios of these melts. The small fraction of the primary melts with elevated MnO/MgO ratios (Fig. 2a) may reflect contributions from unusually MnO-rich slab sediments, although these melts may also

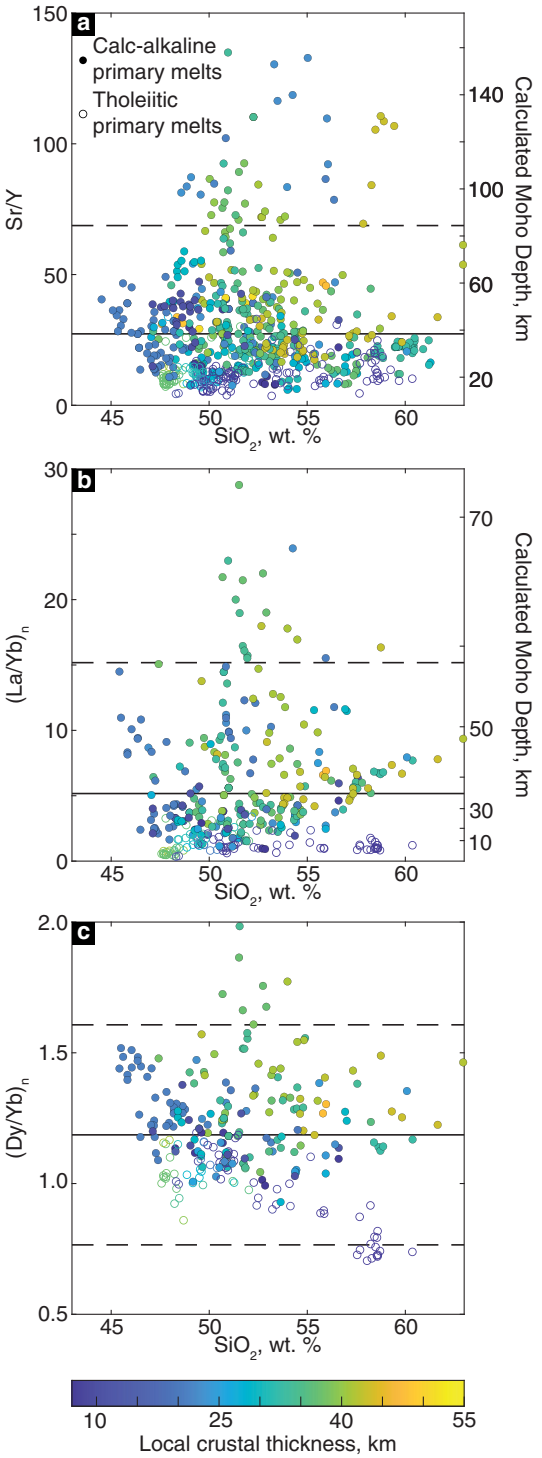

Figure 1 Variations in the trace element ratios of calc-alkaline and tholeiitic primary arc melts compared to SiO_2 (wt. %). In all panels, symbol colours are based on local arc thickness calculated from CRUST1.0 (Laske *et al.*, 2013), and empty symbols show tholeiitic lavas. Mean values are shown with solid black lines and 1 standard deviation is marked with dashed black lines. **(a)** Sr/Y, with equivalent crustal thickness from empirical model in Chapman *et al.* (2015) shown on right hand *y*-axis. **(b)** Chondrite normalised La/Yb, with equivalent crustal thickness calculated using Equation 2 in Profeta *et al.* (2015) shown in right hand *y*-axis. **(c)** Variations in chondrite normalised Dy/Yb ratios. REE ratios in **(b)** and **(c)** normalised to chondritic values from McDonough and Sun (1995).

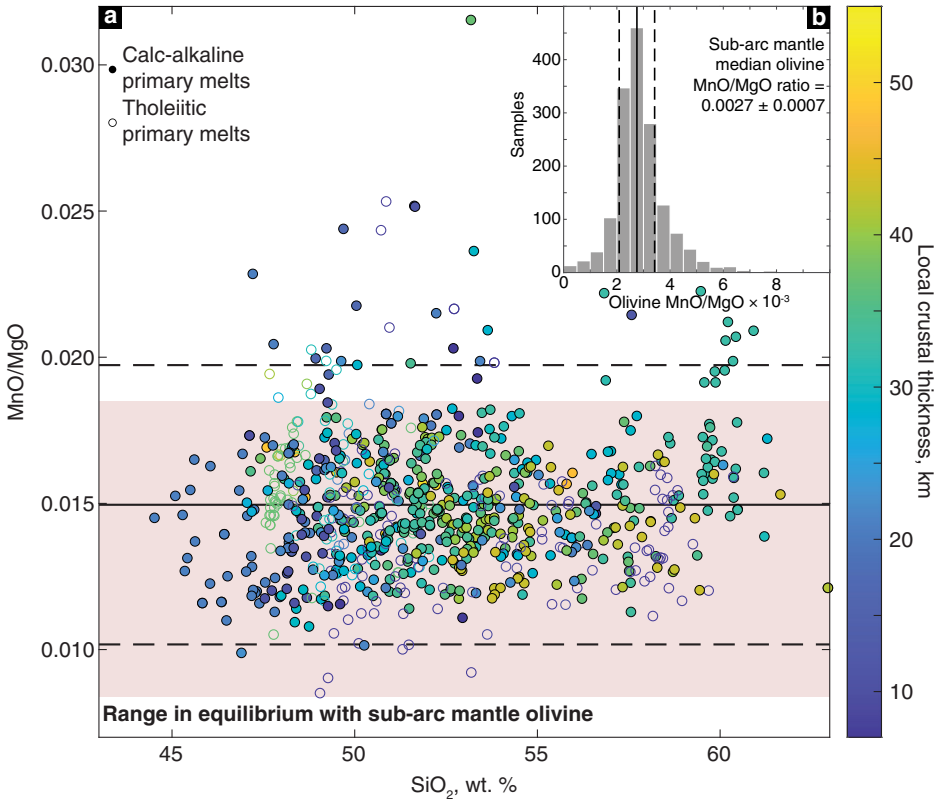

Figure 2 **(a)** Range in MnO/MgO ratios of calc-alkaline and tholeiitic primary arc melts compared to SiO_2 (wt. %). Symbols as in Figure 1: marker colour indicates crustal thickness interpolated from CRUST1.0, with filled symbols used to show calc-alkaline primary melts and empty symbols showing tholeiitic primary melts. Field of MnO/MgO ratios in equilibrium with mantle olivine is shown in pink, and calculated using the model in Blundy *et al.* (2020) and temperatures from 1100 to 1350 °C, olivine forsterite contents from 0.88 to 0.92, and compiled olivine MnO/MgO ratios. **(b)** Histogram of sub-arc mantle olivine MnO/MgO ratios from manually filtered GEOROC (https://georoc.eu/) pre-compiled olivine dataset (DIGIS Team, 2022). Olivine dataset available in Table S-2.

have undergone limited fractionation of olivine ± clinopyroxene (see below).

Methods and Data Compilation

The previous section demonstrates that mantle-derived melts show a restricted range of MnO/MgO ratios that are reflective of equilibration with mantle olivine. To characterise the evolution of this ratio during crystallisation differentiation, we compiled Mn-Mg mineral-melt partitioning data from published experimental studies, focusing on studies that include garnet-bearing experiments. As MnO is commonly included in experimental bulk compositions and is a standard electron microprobe analyte, we were able to compile large datasets of Mn/Mg partition coefficients for all typical experimental phases. The full list of compiled experimental references is available in the Supplementary Information References.

Although commonly measured, MnO is frequently present at <0.1 wt. % concentrations in experimental melts and is only rarely an emphasis of experimental studies (*cf.* Balta *et al.*, 2011). Further, in experiments conducted at relatively low temperatures, garnets can be strongly zoned. Due to these analytical complications, propagated relative uncertainties on experimental Mn/Mg partition coefficients ($K_D^{Mn\text{-}Mg}$) in many experiments, and particularly at lower temperatures and pressures relevant to garnet fractionation, are >50 % (1 standard deviation). To address these limitations, we reanalysed garnet and melt compositions from two previous experimental studies relevant to garnet crystallisation at crustal conditions (Alonso-Perez *et al.*, 2009; Ulmer *et al.*, 2018). We used laser ablation ICP-MS to remeasure melt MnO contents and made new electron microprobe measurements of garnet rim major element contents from 25 experiments. Detailed descriptions of analytical methods are available in the Supplementary Information, and the new analyses are presented in Table S-1. All compiled garnet partitioning data are shown in Figure 3d. As our primary focus here is on the role of garnet in subduction zone magmas, we subsequently exclude experiments conducted at pressures >5 GPa or those containing significant amounts of CO_2 or where the standard deviation uncertainty (1σ) on garnet $K_D^{Mn\text{-}Mg}$ is ≥50 %.

Results and Discussion

Our compiled partitioning data shows that garnet is unique among commonly fractionating minerals: most silicate phases are characterised by $K_D^{Mn\text{-}Mg}$ consistently <1, and typically <0.5 (Fig. 3a–c), while garnet $K_D^{Mn\text{-}Mg}$ shows considerably more variation but is consistently higher than other phases (≥1; Fig. 3d). In contrast to non-garnet silicates, Fe-Ti oxides also typically have $K_D^{Mn\text{-}Mg} > 1$ (Fig. S-2). However, these oxides incorporate much smaller amounts of MnO and MgO compared to garnet and are usually less abundant, and thus their fractionation has a comparatively smaller influence on melt compositions. To better constrain the effect of garnet fractionation, we modelled the garnet-melt $K_D^{Mn\text{-}Mg}$ data using an Arrhenius type function (Fig. 3e). We explored models with additional parameters including melt and garnet compositions, and fO_2, but did not find that incorporating extra variables improved model performance.

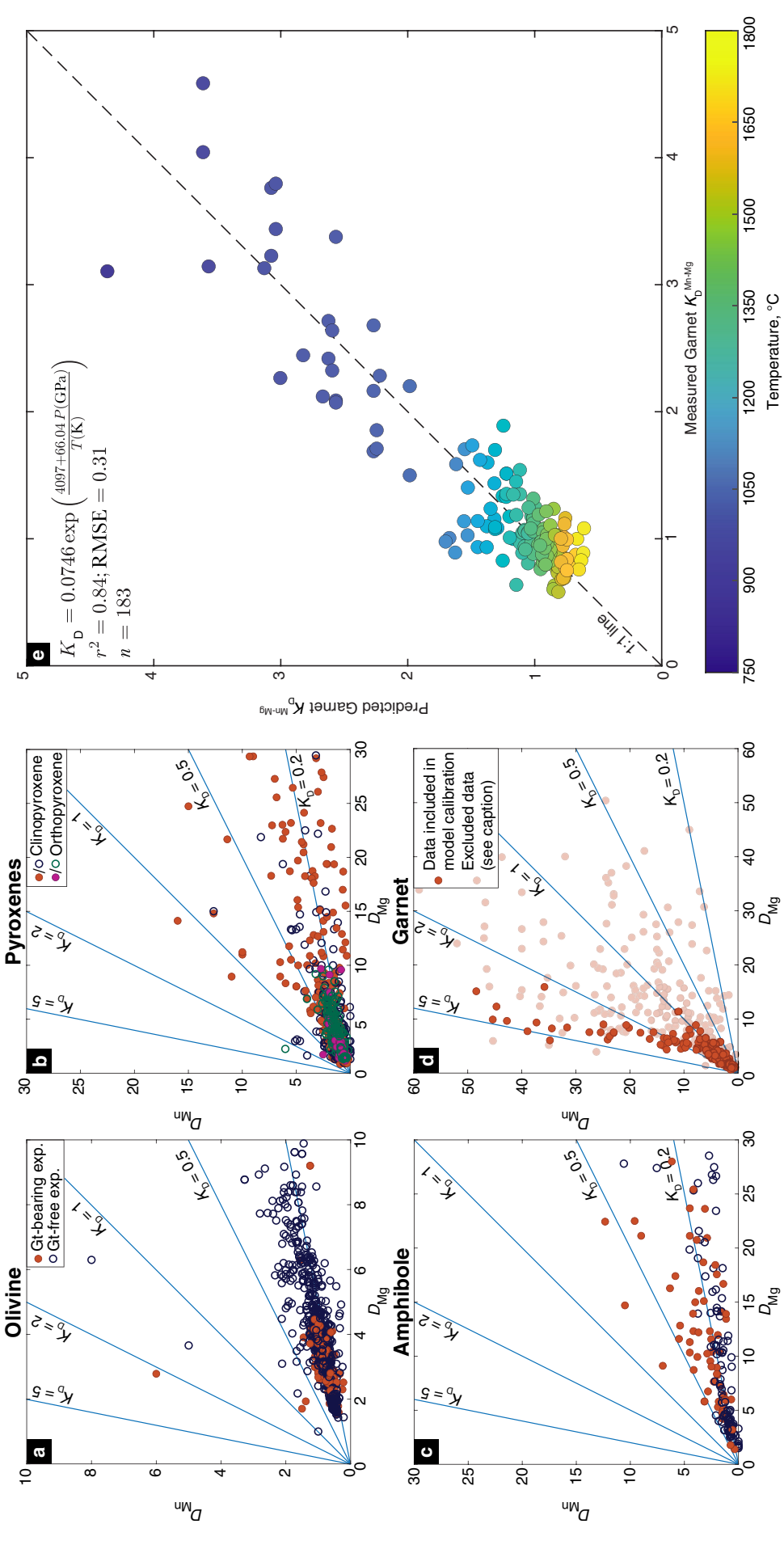

Figure 3 **(a–d)** Compiled experimental Mn and Mg partition coefficients for **(a)** olivine, **(b)** clinopyroxene and orthopyroxene, **(c)** amphibole, and **(d)** garnet. In **(a–c)**, data from garnet-bearing experiments are shown with filled symbols and garnet-free experiments are unfilled. In **(d)**, solid symbols show the garnet data used to model the partitioning behaviour, while excluded data (primarily due to high analytical uncertainties, see text) are semi-transparent. **(e)** Comparison of experimentally measured garnet $K_D^{Mn\text{-}Mg}$ and predicted values. Compiled data used in model calibration are available in Table S-3. References for data compiled and plotted in panels **(a–d)** are listed in the Supplementary Information.

Additional experiments may reveal other variables that influence garnet $K_D^{Mn\text{-}Mg}$. However, given the robust model fit presented here, we expect other variables to be secondary to the effects of changing temperature and pressure.

The distinctive partitioning behaviour of garnet makes MnO/MgO ratios ideal for isolating the impact of garnet fractionation. Unlike MnO/FeO ratios, which were previously used to identify distinct mantle melt source regions (*e.g.*, Balta *et al.*, 2011), the evolution of MnO/MgO ratios are insensitive to variations in magmatic fO_2: while Mn can occur in multiple valence states, the MnO-Mn_3O_4 fO_2 buffer is more than 4 log units above QFM, and thus Mn^{3+} is negligible in typical arc magmas (O'Neill and Pownceby, 1993). In comparison, the partitioning of MnO from total iron will inevitably introduce fO_2 sensitivity due to the significant quantities of Fe^{3+} present at typical magmatic fO_2 conditions. Additionally, apart from fO_2 effects, MnO and FeO are much less strongly partitioned by most silicate phases, significantly complicating the ability to isolate the effects of garnet fractionation with MnO/FeO ratios.

Using our model for garnet $K_D^{Mn\text{-}Mg}$, we can estimate how melt MnO/MgO ratios evolve in response to fractionation of various phases. We find that at pressures <2 GPa, the garnet $K_D^{Mn\text{-}Mg}$ is >1 for any magma below 1300 °C. At conditions more typical to arc lower crust, the garnet $K_D^{Mn\text{-}Mg}$ increases to values >2, and thus pure garnet fractionation will cause melt MnO/MgO ratios to decrease. The effect of garnet fractionation is further amplified when comparing the effect of garnet fractionation in MnO/MgO to SiO_2. As garnet has much lower SiO_2 contents than typical arc melts, garnet fractionation will cause rapid increases in melt SiO_2 while hindering increases in MnO/MgO ratios, a distinctive trend in comparison to most other phases that crystallise from arc melts.

The impact of garnet fractionation is evident when examining the SiO_2 contents and MnO/MgO ratios of typical arc melts (Fig. 4). Clear differences are immediately apparent between relatively thin-crusted island arcs and continental arcs with thicker upper plates. Melts in both settings originate near the primitive arc compositions shown in Figure 2, but island arc magmas rapidly evolve to significantly higher MnO/MgO values, consistent with initial olivine + clinopyroxene dominated fractionation (Fig. 4a). Lavas from the westernmost Aleutian Arc and from Matthew and Hunter Volcanoes in Vanuatu are notable exceptions to the general island arc trend and are highlighted in Figure 4a. Erupted lavas at these locations are generally evolved and have very low MnO/MgO ratios, likely requiring the involvement of garnet in their petrogenesis. This is consistent with independent evidence that supports a slab-derived origin for these magmas (Yogodzinski *et al.*, 2015; McCarthy *et al.*, 2022), and suggests that in rare instances arc lavas retain a garnet-source signature without complete re-equilibration with the mantle wedge.

In contrast to the typical island arc trend, increases in MnO/MgO values at continental arcs are much more limited (Fig. 4b), requiring significant garnet fractionation in addition to olivine ± clinopyroxene. It is particularly noteworthy that this divergent behaviour occurs during early fractionation of basaltic melts. Amphibole and/or Fe-Ti oxides also have low to very low SiO_2 contents and moderate to high $K_D^{Mn\text{-}Mg}$, and thus can also limit the extent of increases in MnO/MgO ratios (Figs. 4, S-2). However, these phases do not crystallise from typical arc melts until cooling to temperatures below at least ~1050 °C and cannot be responsible for the divergent behaviour observed in basaltic compositions. Further, the minimum pressures at which garnet is stable increase for less evolved magmas (Fig. S-3). Early garnet fractionation from basaltic liquids therefore requires that garnet fractionation begins at pressures ≥1.5 GPa, or equivalently ≥50 km depth. Our current data do not allow us to distinguish between ubiquitous garnet fractionation and mixing between deep garnet fractionating magmas and more shallowly differentiating magmas. However, either scenario requires that at least some magmas undergo garnet fractionation at or below the Moho of many continental arcs.

The widespread fractionation of garnet-rich cumulates at or below the Moho in modern continental arcs is difficult to verify with geophysical techniques, as these cumulates have densities and seismic velocities comparable to or greater than

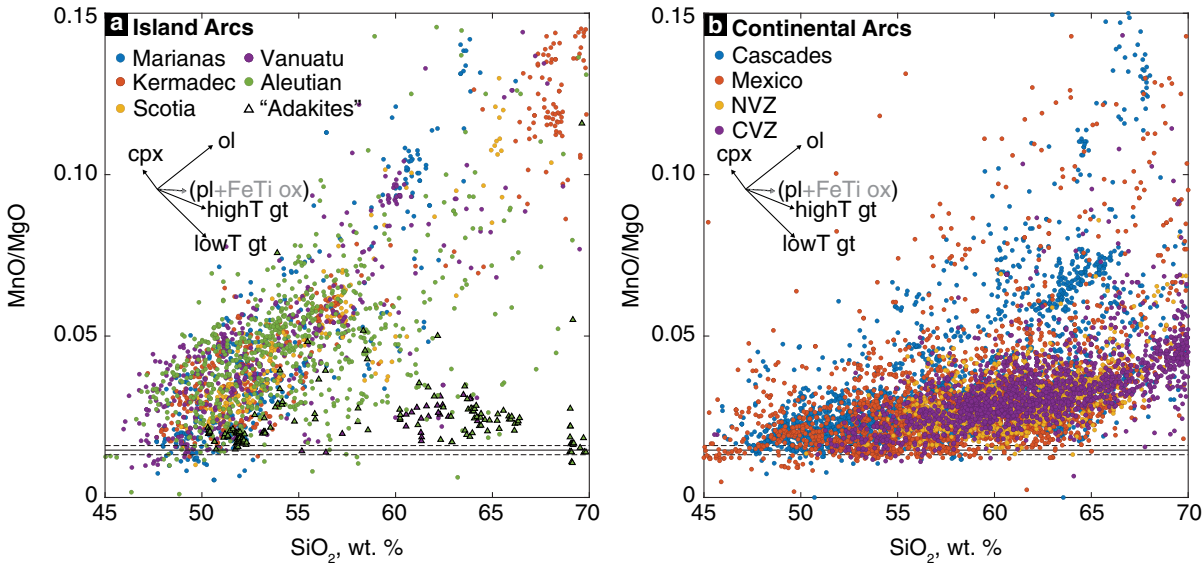

Figure 4 Evolution of MnO/MgO ratios as a function of SiO_2 contents in lavas from representative modern **(a)** island arcs, and **(b)** continental arcs. Previously identified lavas with slab melt signatures from the western Aleutians (Yogodzinski *et al.*, 2015) and Vanuatu (McCarthy *et al.*, 2022) are highlighted with black triangles in **(a)**. In both panels, the mean (solid) and standard deviation MnO/MgO ratios (dashed) of primary arc melts are plotted with black lines, and representative fractionation vectors are calculated for crystallisation of typical phases from near-primary arc basalts. All data downloaded from GEOROC (https://georoc.eu/) precompiled datasets for convergent margins in May 2021 (DIGIS Team, 2022).

sub-arc mantle (Müntener and Ulmer, 2006). Instead, fractionation of these cumulates near the base of the crust may contribute to the commonly poorly defined seismic Moho at many arcs. Finally, while both calc-alkaline (Fe-depletion) and tholeiitic (Fe-enrichment) differentiation sequences are observed at most arcs, calc-alkaline trends appear dominant in the thickest arcs (Chiaradia, 2014). This observation, combined with the findings here, suggests an important role for garnet fractionation in the generation of some calc-alkaline differentiation sequences (*e.g.*, Tang *et al.*, 2018). However, calc-alkaline sequences are produced by extensive crystallisation differentiation that includes other phases such as FeTi oxides and amphibole. The stability of these phases is controlled by variables including fO_2 and magmatic H_2O contents, and thus a range of variables and fractionating assemblages likely combine to drive calc-alkaline differentiation (Sisson and Grove, 1993; Sisson *et al.*, 2005; Zimmer *et al.*, 2010).

Conclusions

On a global scale, trace element ratios such as Sr/Y and La/Yb appear to correlate with arc crustal thickness, and thus may be broadly reflective of varying extents of garnet fractionation. However, applying these proxies to individual magmatic suites can lead to incorrectly inferring garnet fractionation in magmas that instead reflect significant slab components and/or plagioclase accumulation. We show that MnO/MgO ratios avoid many of these limitations and provide a powerful tool to illustrate the role of garnet fractionation. Arc primary melts show a restricted range of MnO/MgO ratios that are consistent with melts in equilibrium with mantle olivine. Further, during early stages of fractionation, garnet is the only crystallising phase that does not drive magmas to evolve to higher MnO/MgO ratios. This diagnostic behaviour appears to be quite common in thicker continental arcs, suggesting that crystallisation differentiation with or without increasing fO_2 begins for many continental arc magmas at or below the Moho.

Acknowledgements

The authors thank P. Ulmer for providing us with experimental charges and M. Robyr and A. Ulyanov for assistance with EPMA and LA-ICP-MS respectively. Tom Sisson and Cin-Ty Lee provided valuable reviews of a previous version of this manuscript. OM acknowledges support from the Swiss National Science Foundation grant number 200021_197258 and BZK acknowledges funding support from the University of Lausanne.

Editor: Ambre Luguet

Additional Information

Supplementary Information accompanies this letter at https://www.geochemicalperspectivesletters.org/article2309.

Cite this letter as: Klein, B.Z., Müntener, O. (2023) MnO/MgO ratios of arc basalts highlight the role of early garnet fractionation. *Geochem. Persp. Let.* 25, 18–24. https://doi.org/10.7185/geochemlet.2309

References

Alonso-Perez, R., Müntener, O., Ulmer, P. (2009) Igneous garnet and amphibole fractionation in the roots of island arcs: experimental constraints on andesitic liquids. *Contributions to Mineralogy and Petrology* 157, 541–558. https://doi.org/10.1007/s00410-008-0351-8

Balta, J.B., Asimow, P.D., Mosenfelder, J.L. (2011) Manganese partitioning during hydrous melting of peridotite. *Geochimica et Cosmochimica Acta* 75, 5819–5833. https://doi.org/10.1016/j.gca.2011.05.026

Blundy, J., Melekhova, E., Ziberna, L., Humphreys, M.C.S., Cerantola, V., Brooker, R.A., McCammon, C.A., Pichavant, M., Ulmer, P. (2020) Effect of redox on Fe–Mg–Mn exchange between olivine and melt and an oxybarometer for basalts. *Contributions to Mineralogy and Petrology* 175, 1–32. https://doi.org/10.1007/s00410-020-01736-7

Chapman, J.B., Ducea, M.N., DeCelles, P.G., Profeta, L. (2015) Tracking changes in crustal thickness during orogenic evolution with Sr/Y: An example from the North American Cordillera. *Geology* 43, 919–922. https://doi.org/10.1130/g36996.1

Chiaradia, M. (2014) Copper enrichments in arc magmas controlled by overriding plate thickness. *Nature Geoscience* 7, 43–46. https://doi.org/10.1038/NGEO2028

Davidson, J., Turner, S., Handley, H., Macpherson, C., Dosseto, A. (2007) Amphibole "sponge" in arc crust? *Geology* 35, 787–790. https://doi.org/10.1130/g23637a.1

DIGIS Team (2022) GEOROC Compilation: Convergent Margins. GRO.data, V5. https://doi.org/10.25625/PVFZCE

Drummond, M.S., Defant, M.J. (1990) A model for trondhjemite-tonalite-dacite genesis and crustal growth via slab melting: Archean to modern comparisons. *Journal of Geophysical Research: Solid Earth* 95, 21503–21521. https://doi.org/10.1029/jb095ib13p21503

Ducea, M.N., Saleeby, J.B. (1996) Buoyancy sources for a large, unrooted mountain range, the Sierra Nevada, California: Evidence from xenolith thermobarometry. *Journal of Geophysical Research: Solid Earth* 101, 8229–8244. https://doi.org/10.1029/95jb03452

Elliott, T. (2004) Tracers of the slab. In: Eiler, J. (Ed.) *Inside the Subduction Factory*. Geophysical Monograph Series 138, American Geophysical Union, Washington D.C., 23–45. https://doi.org/10.1029/138gm03

Grove, T.L., Holbig, E.S., Barr, J.A., Till, C.B., Krawczynski, M.J. (2013) Melts of garnet lherzolite: experiments, models and comparison to melts of pyroxenite and carbonated lherzolite. *Contributions to Mineralogy and Petrology* 166, 887–910. https://doi.org/10.1007/s00410-013-0899-9

Jagoutz, O. (2010) Construction of the granitoid crust of an island arc. Part II: A quantitative petrogenetic model. *Contributions to Mineralogy and Petrology* 160, 359–381. https://doi.org/10.1007/s00410-009-0482-6

Jagoutz, O., Behn, M.D. (2013) Foundering of lower island-arc crust as an explanation for the origin of the continental Moho. *Nature* 504, 131–134. https://doi.org/10.1038/nature12758

Kelley, K.A., Plank, T., Grove, T.L., Stolper, E.M., Newman, S., Hauri, E. (2006) Mantle melting as a function of water content beneath back-arc basins. *Journal of Geophysical Research: Solid Earth* 111, B09208. https://doi.org/10.1029/2005jb003732

Kushiro, I. (1996) Partial Melting of a fertile mantle peridotite at high pressures: An experimental study using aggregates of diamond. In: Basu, A., Hart, S. (Eds.) *Earth Processes: Reading the Isotopic Code*. Geophysical Monograph Series 95, American Geophysical Union, Washington D.C., 109–122. https://doi.org/10.1029/gm095p0109

Laske, G., Masters, G., Ma, Z., Pasyanos, M. (2013) Update on CRUST1.0 - A 1-degree global model of Earth's crust. *Geophysical Research Abstracts* 15, EGU General Assembly, 7–12 April 2013, Vienna, Austria, EGU2013-2658. https://meetingorganizer.copernicus.org/EGU2013/EGU2013-2658.pdf

McCarthy, A., Falloon, T.J., Danyushevsky, L.V., Sauermilch, I., Patriat, M., Jean, M.M., Maas, R., Woodhead, J.D., Yogodzinski, G.M. (2022) Implications of high-Mg# adakitic magmatism at Hunter Ridge for arc magmatism of the Fiji - Vanuatu region. *Earth and Planetary Science Letters* 590, 117592. https://doi.org/10.1016/j.epsl.2022.117592

McDonough, W.F., Sun, S.S. (1995) The composition of the Earth. *Chemical Geology* 120, 223–253. https://doi.org/10.1016/0009-2541(94)00140-4

Müntener, O., Ulmer, P. (2006) Experimentally derived high-pressure cumulates from hydrous arc magmas and consequences for the seismic velocity structure of lower arc crust. *Geophysical Research Letters* 33, L21308. https://doi.org/10.1029/2006gl027629

O'Neill, H.St.C., Pownceby, M.I. (1993) Thermodynamic data from redox reactions at high temperatures. II. The MnO–Mn_3O_4 oxygen buffer, and implications for the thermodynamic properties of MnO and Mn_3O_4. *Contributions to Mineralogy and Petrology* 114, 315–320. https://doi.org/10.1007/bf01046534

Perrin, A., Goes, S., Prytulak, J., Davies, D.R., Wilson, C., Kramer, S. (2016) Reconciling mantle wedge thermal structure with arc lava thermobarometric determinations in oceanic subduction zones. *Geochemistry, Geophysics, Geosystems* 17, 4105–4127. https://doi.org/10.1002/2016gc006527

Plank, T. (2014) 4.17 - The chemical composition of subducting sediments. In: Holland, H.D., Turekian, K.K. (Eds.) *Treatise on Geochemistry.* Second Edition, Elsevier, Amsterdam, 607–629. https://doi.org/10.1016/b978-0-08-095975-7.00319-3

Profeta, L., Ducea, M.N., Chapman, J.B., Paterson, S.R., Gonzales, S.M.H., Kirsch, M., Petrescu, L., DeCelles, P.G. (2015) Quantifying crustal thickness over time in magmatic arcs. *Scientific Reports* 5, 17786. https://doi.org/10.1038/srep17786

Schmidt, M.W., Jagoutz, O. (2017) The global systematics of primitive arc melts. *Geochemistry, Geophysics, Geosystems* 18, 2817–2854. https://doi.org/10.1002/2016gc006699

Schmidt, M.W., Vielzeuf, D., Auzanneau, E. (2004) Melting and dissolution of subducting crust at high pressures: the key role of white mica. *Earth and Planetary Science Letters* 228, 65–84. https://doi.org/10.1016/j.epsl.2004.09.020

Sisson, T.W., Grove, T.L. (1993) Experimental investigations of the role of H_2O in calc-alkaline differentiation and subduction zone magmatism. *Contributions to Mineralogy and Petrology* 113, 143–166. https://doi.org/10.1007/bf00283225

Sisson, T.W., Ratajeski, K., Hankins, W.B., Glazner, A.F. (2005) Voluminous granitic magmas from common basaltic sources. *Contributions to Mineralogy and Petrology* 148, 635–661. https://doi.org/10.1007/s00410-004-0632-9

Tang, M., Erdman, M., Eldridge, G., Lee, C.-T.A. (2018) The redox "filter" beneath magmatic orogens and the formation of continental crust. *Science Advances* 4, eaar4444. https://doi.org/10.1126/sciadv.aar4444

Ulmer, P., Kaegi, R., Müntener, O. (2018) Experimentally derived intermediate to silica-rich arc magmas by fractional and equilibrium crystallization at 1.0 GPa: An evaluation of phase relationships, compositions, liquid lines of descent and oxygen fugacity. *Journal of Petrology* 59, 11–58. https://doi.org/10.1093/petrology/egy017

Vukadinovic, D. (1993) Are Sr enrichments in arc basalts due to plagioclase accumulation? *Geology* 21, 611–614. https://doi.org/10.1130/0091-7613(1993)021< 0611:aseiab> 2.3.co;2

Walter, M.J. (1998) Melting of garnet peridotite and the origin of komatiite and depleted lithosphere. *Journal of Petrology* 39, 29–60. https://doi.org/10.1093/petroj/39.1.29

Yogodzinski, G.M., Brown, S.T., Kelemen, P.B., Vervoort, J.D., Portnyagin, M., Sims, K.W.W., Hoernle, K., Jicha, B.R., Werner, R. (2015) The role of subducted basalt in the source of island arc magmas: Evidence from seafloor lavas of the Western Aleutians. *Journal of Petrology* 56, 441–492. https://doi.org/10.1093/petrology/egv006

Zimmer, M.M., Plank, T., Hauri, E.H., Yogodzinski, G.M., Stelling, P., Larsen, J., Singer, B., Jicha, B., Mandeville, C., Nye, C.J. (2010) The role of water in generating the calc-alkaline trend: New volatile data for Aleutian magmas and a new Tholeiitic Index. *Journal of Petrology* 51, 2411–2444. https://doi.org/10.1093/petrology/egq062

Geochemical Perspectives Letters

MnO/MgO ratios of arc basalts highlight the role of early garnet fractionation

B.Z. Klein, O. Müntener

Supplementary Information

The Supplementary Information includes:

- Analytical Methods
- Tables S-1 to S-3
- Figures S-1 to S-4
- Data References for Figures 3 and S-2
- Supplementary Information References

Analytical Methods

New electron microprobe measurements of experimental garnets. New analyses of garnet major element contents from previously published experiments (Alonso-Perez *et al*., 2009; Ulmer *et al*., 2018) were made using the JEOL JXA-8530F field emission gun electron probe microanalyser (EPMA) housed in the Institute of Earth Sciences at the University of Lausanne. Analyses were performed using a 15 kV accelerating voltage, a 20 nA beam current and a focused electron beam. All elements were measured using 30 second on-peak counting times and 10 second off-peak background measurements. Calibration standards used for analysed elements included wollastonite (Si and Ca), ilmenite (Ti), andalusite (Al), fayalite (Fe), tephrite (Mn), forsterite (Mg), and albite (Na). As some of the experimental garnets were found to be strongly zoned, special efforts were made to include only analyses within ~5 μm of garnet rims. Raw data were corrected for matrix effects using the CITZAF package (Armstrong, 1995).

New Laser Ablation ICP-MS measurements of experimental glasses. New analyses of experimental glass MnO contents from the same set of experiments were collected using a RESOlution SE 193 nm Ar-F excimer ablation system equipped with an S155 2-volume ablation cell (ASI, Australia) coupled to an Element XR sector field ICP-MS at the Institute of Earth Sciences at the University of Lausanne. Laser ablation was performed using a 30 μm laser spot size and 10 Hz repetition rate, and an energy density of 5 J/cm^2. Analyses were standardised using glass standard BCR-2G (GeoREM). ^{57}Fe was used for internal standardisation. Glass standard NIST SRM 610 was regularly analysed as a secondary standard and produced a mean MnO concentration of 0.0567 ± 0.0006 wt. %, in agreement with the published composition of 0.057 ± 0.002 wt. % (Jochum *et al*., 2011). Analyses of unknowns were made in triplicate and offline data reduction was performed using LAMTRACE (Jackson, 2008). Experiment RP33 from Alonso-Perez *et al*. (2009) did not contain melt pockets large enough for analysis by laser ablation ICP-MS, and for this sample we re-analysed the glass MnO composition by EPMA. For the most part, new analyses agree within uncertainty with published EPMA analyses, but have significantly lower uncertainties (Fig. S-4).

Supplementary Tables

Table S-1 Tables of new and previously published MnO and MgO concentrations for experimental glasses and garnets from experiments in Alonso-Perez *et al*. (2009) and Ulmer *et al.* (2018): (a) new experimental glass MnO concentrations measured with LA-ICP-MS compared to original published concentrations measured by EPMA; and (b) new and published experimental garnet compositions, both measured by EPMA.

Table S-2 Compilation of sub-arc mantle olivine compositions. Dataset is based on GEOROC (https://georoc.eu/) precompiled olivine dataset (DIGIS Team, 2022; downloaded Nov. 9, 2021), and was manually filtered to only include analyses of primary sub-arc mantle olivine compositions, with MnO concentrations reported and analytical totals between 98–102 wt. %. Data references are listed on the second sheet of the table.

Table S-3 Detailed information for experiments used in garnet $K_D^{Mn\text{-}Mg}$ model calibration.

Tables S-1 through S-3 (.xlsx) are available for download from the online version of this article at https://doi.org/10.7185/geochemlet.2309.

Supplementary Figures

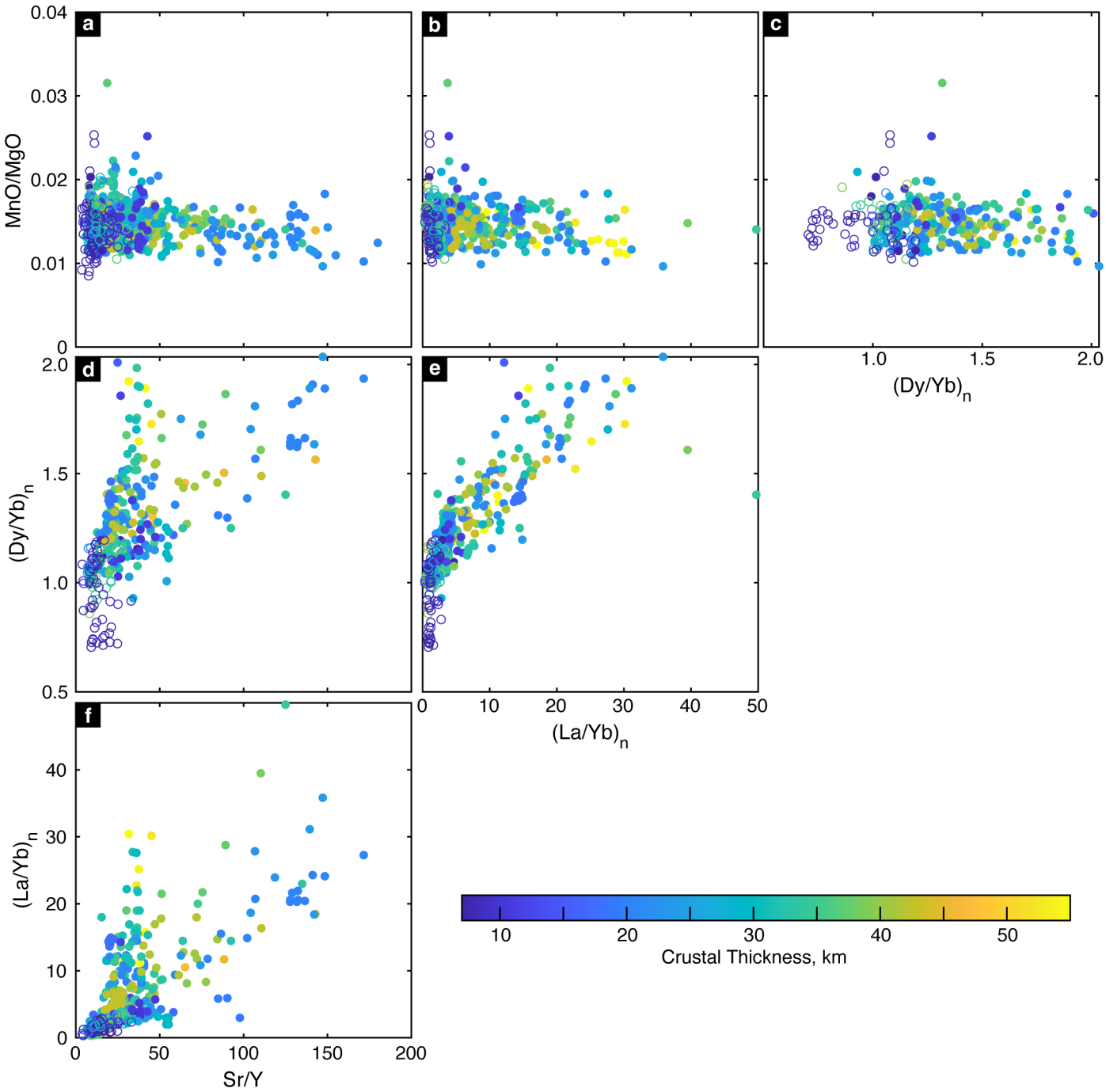

Figure S-1 Plot matrix comparing trace element proxies for crustal thickness and MnO/MgO ratios. **(a–c)** Comparisons of MnO/MgO ratios to trace element proxies. MnO/MgO ratios are uncorrelated with all three trace element ratios. **(d–f)** Comparisons between trace element proxies, showing strong correlations between proxies. Symbols as in Figure 1: marker colour corresponds to local crustal thickness interpolated from CRUST1.0, and empty symbols show tholeiitic lavas while filled symbols are used for calc-alkaline lavas.

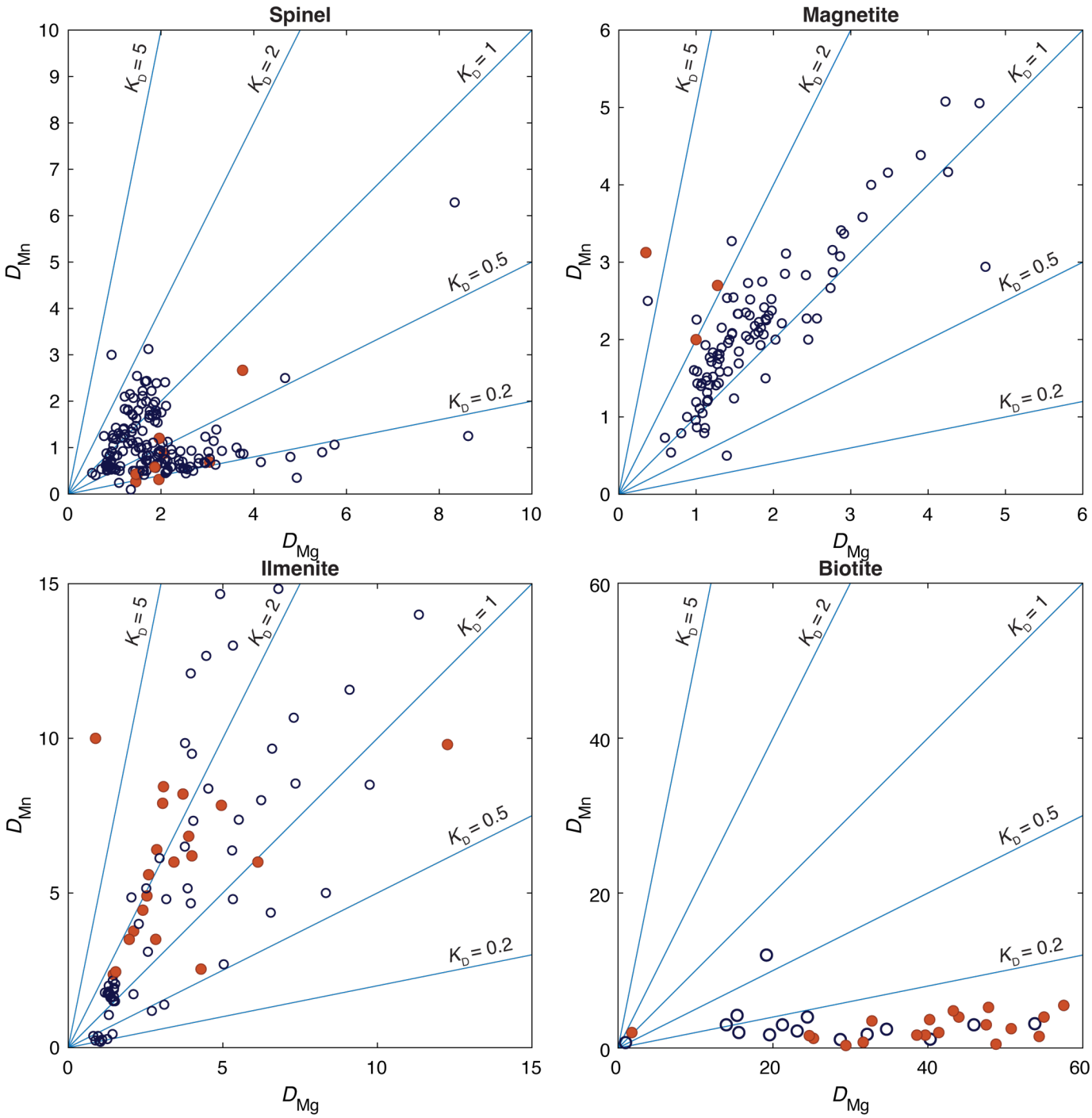

Figure S-2 Compiled experimental Mn and Mg partition coefficients for additional phases: **(a)** spinel (including chromian and hercynitic spinels), **(b)** magnetite, **(c)** ilmenite and **(d)** biotite. Data from garnet-bearing experiments are shown with filled symbols and garnet-free experiments are unfilled. The experimental studies included in this compilation are listed in the next section, "Data References for Figures 3 and S-2".

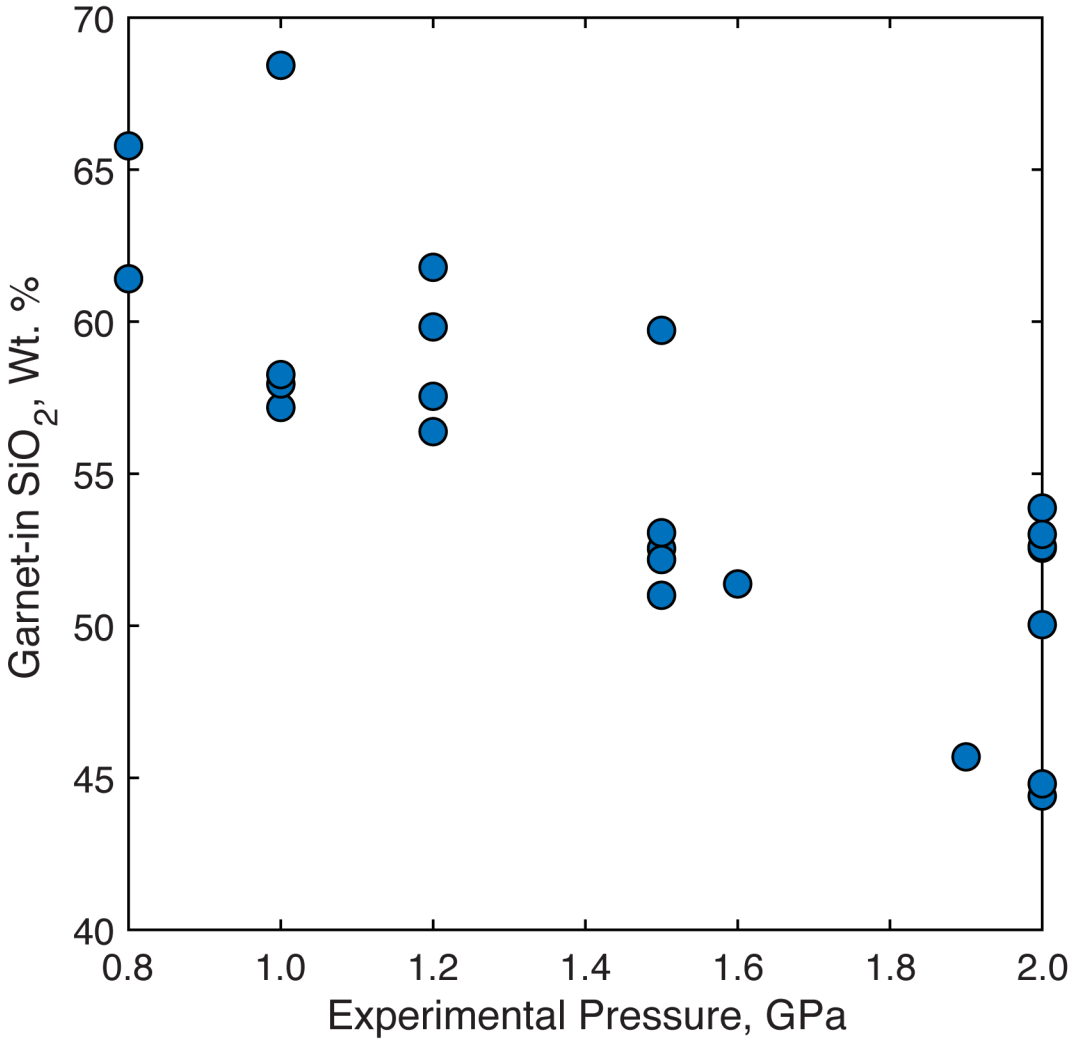

Figure S-3 Comparison of pressure and melt composition controls on experimental garnet stability. Points show minimum melt SiO_2 contents when garnet first joins crystallising assemblage for each series of experiments conducted for one starting composition at constant pressure and varying temperatures. Note that most of these experiments do not represent true liquidus garnet, and that liquidus garnet requires more evolved melt compositions at a given pressure than what is shown here. Experiments plotted include: Draper and Johnston, 1992; Vander Auwera and Longhi, 1994; Wolf and Wyllie, 1994; Skjerlie and Johnston, 1996; Kinzler, 1997; Müntener *et al.*, 2001; Hirschmann *et al.*, 2003; Pertermann and Hirschmann, 2003; Keshav *et al.*, 2004; Alonso-Perez, 2007; Mercer and Johnston, 2008; Alonso-Perez *et al.*, 2009; Ulmer *et al.*, 2018.

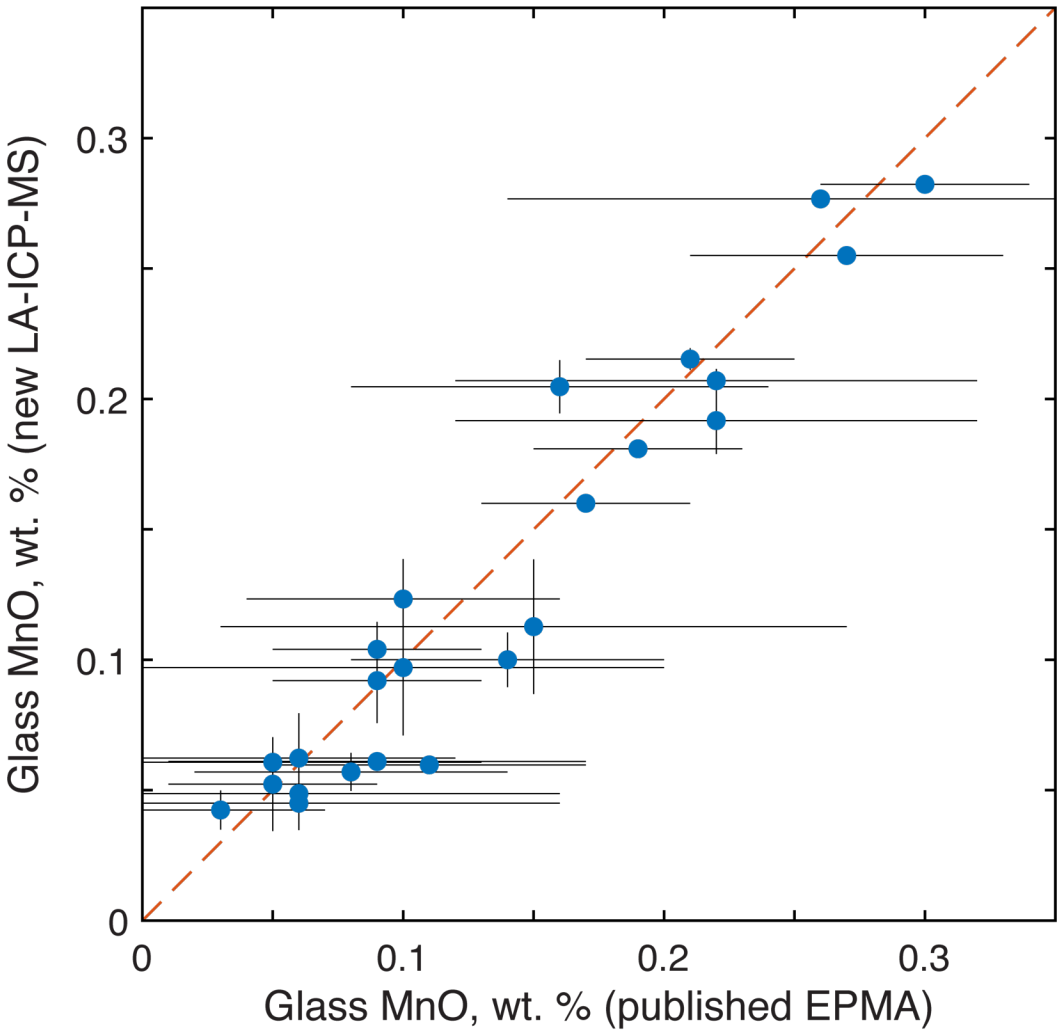

Figure S-4 Comparison of published experimental glass MnO contents measured with EPMA from Alonso-Perez *et al*. (2009) and Ulmer *et al*. (2018) to new LA-ICP-MS measured glass MnO contents. Error bars show two standard deviation measurement uncertainties. In most experiments, measurements agree within uncertainty, but new LA-ICP-MS uncertainties are significantly reduced compared to published EPMA data.

Data References for Figures 3 and S-2

Data sources used in Figures 3 and S-2 and already included in the Supplementary Reference List (next section): Ackerson *et al*. (2017), Agee and Draper (2004), Alonso-Perez (2007), Alonso-Perez *et al*. (2009), Aubaud *et al*. (2008), Balta *et al*. (2011), Condamine *et al*. (2016), Cruz-Uribe *et al*. (2018), Davis and Hirschmann (2013), Davis et *al*. (2013), Draper and Johnston (1992), Draper *et al*. (2006), Gaetani and Grove (1998, 2003), Grove *et al*. (2013), Hirschmann *et al*. (2003), Holbig and Grove (2008), Johnston (1986), Keshav *et al*. (2004), Kinzler (1997), Kogiso and Hirschmann (2006), Kogiso *et al*. (2003), Longhi (1995, 2002), Mercer and Johnston (2008), Müntener *et al*. (2001), Parman and Grove (2004), Pertermann and Hirschmann (2003), Skjerlie and Johnston (1996), Tenner *et al*. (2012), Ulmer *et al.* (2018), Vander Auwera and Longhi (1994), Walter (1998).

Additional data sources used in Figures 3 and S-2:

Baasner, A., Médard, E., Laporte, D., Hoffer, G. (2016) Partial melting of garnet lherzolite with water and carbon dioxide at 3 GPa using a new melt extraction technique: implications for intraplate magmatism. *Contributions to Mineralogy and Petrology* 171, 45. https://doi.org/10.1007/s00410-016-1233-0

Carroll, M.R., Wyllie, P.J. (1989) Experimental Phase Relations in the System Tonalite-Peridotite-H_2O at 15 kb; Implications for Assimilation and Differentiation Processes near the Crust-Mantle Boundary. *Journal of Petrology* 30, 1351–1382. https://doi.org/10.1093/petrology/30.6.1351

Chen, H.-K., Delano, J.W., Lindsley, D.H. (1982) Chemistry and phase relations of VLT Volcanic glasses from Apollo 14 and Apollo 17. *Journal of Geophysical Research: Solid Earth* 87, A171–A181. https://doi.org/10.1029/jb087is01p0a171

Dasgupta, R., Hirschmann, M.M., Smith, N.D. (2007) Partial Melting Experiments of Peridotite + CO_2 at 3 GPa and Genesis of Alkalic Ocean Island Basalts. *Journal of Petrology* 48, 2093–2124. https://doi.org/10.1093/petrology/egm053

Delano, J.W. (1977) Experimental melting relations of 63545, 76015, and 76055. *Proceedings of the 8th Lunar Science Conference*, 14–18 March 1977, Houston, TX, 2097–2123. https://articles.adsabs.harvard.edu/pdf/1977LPSC....8.2097D

Draper, D.S., Green, T.H. (1997) P–T Phase Relations of Silicic, Alkaline, Aluminous Mantle-Xenolith Glasses Under Anhydrous and C–O–H Fluid-saturated Conditions. *Journal of Petrology* 38, 1187–1224. https://doi.org/10.1093/petroj/38.9.1187

Draper, D.S., Xirouchakis, D., Agee, C.B. (2003) Trace element partitioning between garnet and chondritic melt from 5 to 9 GPa: implications for the onset of the majorite transition in the martian mantle. *Physics of the Earth and Planetary Interiors* 139, 149–169. https://doi.org/10.1016/s0031-9201(03)00150-x

Elkins-Tanton, L.T., Grove, T.L. (2003) Evidence for deep melting of hydrous metasomatized mantle: Pliocene high-potassium magmas from the Sierra Nevadas. *Journal of Geophysical Research: Solid Earth* 108, 2350. https://doi.org/10.1029/2002jb002168

Elkins-Tanton, L.T., Draper, D.S., Agee, C.B., Jewell, J., Thorpe, A., Hess, P.C. (2007) The last lavas erupted during the main phase of the Siberian flood volcanic province: results from experimental petrology. *Contributions to Mineralogy and Petrology* 153, 191–209. https://doi.org/10.1007/s00410-006-0140-1

Ernst, W.G., Liu, J. (1998) Experimental phase-equilibrium study of Al- and Ti-contents of calcic amphibole in MORB—A semiquantitative thermobarometer. *American Mineralogist* 83, 952–969. https://doi.org/10.2138/am-1998-9-1004

Gerbode, C., Dasgupta, R. (2010) Carbonate-fluxed Melting of MORB-like Pyroxenite at 2.9 GPa and Genesis of HIMU Ocean Island Basalts. *Journal of Petrology* 51, 2067–2088. https://doi.org/10.1093/petrology/egq049

Hermann, J., Spandler, C.J. (2008) Sediment Melts at Sub-arc Depths: an Experimental Study. *Journal of Petrology* 49, 717–740. https://doi.org/10.1093/petrology/egm073

Inoue, T., Rapp, R.P., Zhang, J., Gasparik, T., Weidner, D.J., Irifune, T. (2000) Garnet fractionation in a hydrous magma ocean and the origin of Al-depleted komatiites: melting experiments of hydrous pyrolite with REEs at high pressure. *Earth and Planetary Science Letters* 177, 81–87. https://doi.org/10.1016/s0012-821x(00)00038-8

Johnson, K.T.M. (1998) Experimental determination of partition coefficients for rare earth and high-field-strength elements between clinopyroxene, garnet, and basaltic melt at high pressures. *Contributions to Mineralogy and Petrology* 133, 60–68. https://doi.org/10.1007/s004100050437

Johnson, M.C., Plank, T. (2000) Dehydration and melting experiments constrain the fate of subducted sediments. *Geochemistry, Geophysics, Geosystems* 1, 1007. https://doi.org/10.1029/1999gc000014

Kjarsgaard, B.A. (1998) Phase relations of a Carbonated High-CaO Nephelinite at 0.2 and 0.5 GPa. *Journal of Petrology* 39, 2061–2075. https://doi.org/10.1093/petroj/39.11-12.2061

Klein, M., Stosch, H.-G., Seck, H.A., Shimizu, N. (2000) Experimental partitioning of high field strength and rare earth elements between clinopyroxene and garnet in andesitic to tonalitic systems. *Geochimica et Cosmochimica Acta* 64, 99–115. https://doi.org/10.1016/s0016-7037(99)00178-7

Klemme, S., Blundy, J.D., Wood, B.J. (2002) Experimental constraints on major and trace element partitioning during partial melting of eclogite. *Geochimica et Cosmochimica Acta* 66, 3109–3123. https://doi.org/10.1016/s0016-7037(02)00859-1

Koester, E., Pawley, A.R., Fernandes, L.A.D., Porcher, C.C., Soliani Jr., E. (2002) Experimental Melting of Cordierite Gneiss and the Petrogenesis of Syntranscurrent Peraluminous Granites in Southern Brazil. *Journal of Petrology* 43, 1595–1616. https://doi.org/10.1093/petrology/43.8.1595

Kogiso, T., Hirose, K., Takahashi, E. (1998) Melting experiments on homogeneous mixtures of peridotite and basalt: application to the genesis of ocean island basalts. *Earth and Planetary Science Letters* 162, 45–61. https://doi.org/10.1016/s0012-821x(98)00156-3

Liu, T.C., Chen, B.R., Chen, C.H. (2000) Melting experiment of a Wannienta basalt in the Kuanyinshan area, northern Taiwan, at pressures up to 2.0 GPa. *Journal of Asian Earth Sciences* 18, 519–531. https://doi.org/10.1016/S1367-9120(00)00002-X

Maner IV, J.L., London, D., Icenhower, J.P. (2019) Enrichment of manganese to spessartine saturation in granite-pegmatite systems. *American Mineralogist* 104, 1625–1637. https://doi.org/10.2138/am-2019-6938

Mengel, K., Green, D.H. (1989) Stability of amphibole and phlogopite in metasomatized peridotite under water-saturated and water-undersaturated conditions. In: Ross, J. (Ed.) *Kimberlites And Related Rocks*, Geological Society of Australia Special Publication 14, Blackwell Scientific, Oxford, 571–581.

Nielsen, R., Ustunisik, G. (2019a) Amphibole/melt partition coefficient experiments v.2. *Interdisciplinary Earth Data Alliance (IEDA)*. https://doi.org/org/10.26022/IEDA/112324

Nielsen, R., Ustunisik, G. (2019b) Clinopyroxene/melt partition coefficient experiments v.2. *Interdisciplinary Earth Data Alliance (IEDA)*. https://doi.org/org/10.26022/IEDA/112325

Nielsen, R., Ustunisik, G. (2019c) Garnet/melt partition coefficient experiments v.2. *Interdisciplinary Earth Data Alliance (IEDA)*. https://doi.org/org/10.26022/IEDA/112323

Nielsen, R., Ustunisik, G. (2019d) Olivine/melt partition coefficient experiments. *Interdisciplinary Earth Data Alliance (IEDA)*. https://doi.org/10.1594/IEDA/111285

Nielsen, R., Ustunisik, G. (2019e) Orthopyroxene/melt partition coefficient experiments. *Interdisciplinary Earth Data Alliance (IEDA)*. https://doi.org/10.1594/IEDA/111289

Nielsen, R., Ustunisik, G. (2019f) Plagioclase/melt partition coefficient experiments. *Interdisciplinary Earth Data Alliance (IEDA)*. https://doi.org/10.1594/IEDA/111284

Nielsen, R., Ustunisik, G. (2019g) Spinel/melt partition coefficient experiments. *Interdisciplinary Earth Data Alliance (IEDA)*. https://doi.org/10.1594/IEDA/111287

Patiño Douce, A.E. (1995) Experimental generation of hybrid silicic melts by reaction of high-Al basalt with metamorphic rocks. *Journal of Geophysical Research: Solid Earth* 100, 15623–15639. https://doi.org/10.1029/94jb03376

Patiño Douce, A.E. (2005) Vapor-Absent Melting of Tonalite at 15–32 kbar. *Journal of Petrology* 46, 275–290. https://doi.org/10.1093/petrology/egh071

Patiño Douce, A.E., Beard, J.S. (1995) Dehydration-melting of Biotite Gneiss and Quartz Amphibolite from 3 to 15 kbar. *Journal of Petrology* 36, 707–738. https://doi.org/10.1093/petrology/36.3.707

Patiño Douce, A.E., Harris, N. (1998) Experimental Constraints on Himalayan Anatexis. *Journal of Petrology* 39, 689–710. https://doi.org/10.1093/petroj/39.4.689

Putirka, K. (1998) Garnet + liquid equilibrium. *Contributions to Mineralogy and Petrology* 131, 273–288. https://doi.org/10.1007/s004100050393

Rapp, R.P., Watson, E.B. (1995) Dehydration Melting of Metabasalt at 8–32 kbar: Implications for Continental Growth and Crust-Mantle Recycling. *Journal of Petrology* 36, 891–931. https://doi.org/10.1093/petrology/36.4.891

Rushmer, T. (1993) Experimental high-pressure granulites: Some applications to natural mafic xenolith suites and Archean granulite terranes. *Geology* 21, 411–414. https://doi.org/10.1130/0091-7613(1993)021<0411:ehpgsa>2.3.co;2

Salters, V.J.M., Longhi, J. (1999) Trace element partitioning during the initial stages of melting beneath mid-ocean ridges. *Earth and Planetary Science Letters* 166, 15–30. https://doi.org/10.1016/s0012-821x(98)00271-4

Sato, K., Katsura, T., Ito, E. (1997) Phase relations of natural phlogopite with and without enstatite up to 8 GPa: implication for mantle metasomatism. *Earth and Planetary Science Letters* 146, 511–526. https://doi.org/10.1016/s0012-821x(96)00246-4

Sisson, T.W., Kelemen, P.B. (2018) Near-solidus melts of MORB + 4 wt% H_2O at 0.8–2.8 GPa applied to issues of subduction magmatism and continent formation. *Contributions to Mineralogy and Petrology* 173, 70. https://doi.org/10.1007/s00410-018-1494-x

Skjerlie, K.P., Patiño Douce, A.E. (2002) The Fluid-absent Partial Melting of a Zoisite-bearing Quartz Eclogite from 1.0 to 3.2 GPa; Implications for Melting in Thickened Continental Crust and for Subduction-zone Processes. *Journal of Petrology* 43, 291–314. https://doi.org/10.1093/petrology/43.2.291

Springer, W., Seck, H.A. (1997) Partial fusion of basic granulites at 5 to 15 kbar: implications for the origin of TTG magmas. *Contributions to Mineralogy and Petrology* 127, 30–45. https://doi.org/10.1007/s004100050263

Suzuki, T., Akaogi, M., Nakamura, E. (2000) Partitioning of major elements between garnet-structured minerals and silicate melt at pressure of 3–15 GPa. *Physics of the Earth and Planetary Interiors* 120, 79–92. https://doi.org/10.1016/s0031-9201(00)00144-8

Tsuno, K., Dasgupta, R. (2011) Melting phase relation of nominally anhydrous, carbonated pelitic-eclogite at 2.5–3.0 GPa and deep cycling of sedimentary carbon. *Contributions to Mineralogy and Petrology* 161, 743–763. https://doi.org/10.1007/s00410-010-0560-9

Tsuno, K., Dasgupta, R. (2012) The effect of carbonates on near-solidus melting of pelite at 3 GPa: Relative efficiency of H_2O and CO_2 subduction. *Earth and Planetary Science Letters* 319–320, 185–196. https://doi.org/10.1016/j.epsl.2011.12.007

Tsuruta, K., Takahashi, E. (1998) Melting study of an alkali basalt JB-1 up to 12.5 GPa: behavior of potassium in the deep mantle. *Physics of the Earth and Planetary Interiors* 107, 119–130. https://doi.org/10.1016/s0031-9201(97)00130-1

Tuff, J., Takahashi, E., Gibson, S.A. (2005) Experimental Constraints on the Role of Garnet Pyroxenite in the Genesis of High-Fe Mantle Plume Derived Melts. *Journal of Petrology* 46, 2023–2058. https://doi.org/10.1093/petrology/egi046

Ulmer, P., Sweeney, R.J. (2002) Generation and differentiation of group II kimberlites: constraints from a high-pressure experimental study to 10 GPa. *Geochimica et Cosmochimica Acta* 66, 2139–2153. https://doi.org/10.1016/s0016-7037(02)00898-0

Supplementary Information References

Ackerson, M.R., Watson, E.B., Tailby, N.D., Spear, F.S. (2017) Experimental investigation into the substitution mechanisms and solubility of Ti in garnet. *American Mineralogist* 102, 158–172. https://doi.org/10.2138/am-2017-5632

Agee, C.B., Draper, D.S. (2004) Experimental constraints on the origin of Martian meteorites and the composition of the Martian mantle. *Earth and Planetary Science Letters* 224, 415–429. https://doi.org/10.1016/j.epsl.2004.05.022

Alonso-Perez, R. (2007) The role of garnet in the evolution of hydrous, calc-alkaline magmas: an experimental study at 0.8–1.5 GPa. PhD Thesis, ETH Zurich, Switzerland. https://doi.org/10.3929/ethz-a-005414579

Alonso-Perez, R., Müntener, O., Ulmer, P. (2009) Igneous garnet and amphibole fractionation in the roots of island arcs: experimental constraints on andesitic liquids. *Contributions to Mineralogy and Petrology* 157, 541–558. https://doi.org/10.1007/s00410-008-0351-8

Armstrong, J.T. (1995) CITZAF: A Package of Correction Programs for the Quantitative Electron Microbeam X-ray Analysis of Thick Polished Materials, Thin Films, and Particles. *Microbeam Analysis* 4, 177–200.

Aubaud, C., Hirschmann, M.M., Withers, A.C., Hervig, R.L. (2008) Hydrogen partitioning between melt, clinopyroxene, and garnet at 3 GPa in a hydrous MORB with 6 wt.% H_2O. *Contributions to Mineralogy and Petrology* 156, 607–625. https://doi.org/10.1007/s00410-008-0304-2

Balta, J.B., Asimow, P.D., Mosenfelder, J.L. (2011) Manganese partitioning during hydrous melting of peridotite. *Geochimica et Cosmochimica Acta* 75, 5819–5833. https://doi.org/10.1016/j.gca.2011.05.026

Condamine, P., Médard, E., Devidal, J.-L. (2016) Experimental melting of phlogopite-peridotite in the garnet stability field. *Contributions to Mineralogy and Petrology* 171, 95. https://doi.org/10.1007/s00410-016-1306-0

Cruz-Uribe, A.M., Marschall, H.R., Gaetani, G.A., Le Roux, V. (2018) Generation of alkaline magmas in subduction zones by partial melting of mélange diapirs—An experimental study. *Geology* 46, 343–346. https://doi.org/10.1130/g39956.1

Davis, F.A., Hirschmann, M.M. (2013) The effects of K_2O on the compositions of near-solidus melts of garnet peridotite at 3 GPa and the origin of basalts from enriched mantle. *Contributions to Mineralogy and Petrology* 166, 1029–1046. https://doi.org/10.1007/s00410-013-0907-0

Davis, F.A., Humayun, M., Hirschmann, M.M., Cooper, R.S. (2013) Experimentally determined mineral/melt partitioning of first-row transition elements (FRTE) during partial melting of peridotite at 3 GPa. *Geochimica et Cosmochimica Acta* 104, 232–260. http://doi.org/10.1016/j.gca.2012.11.009

DIGIS Team (2022) GEOROC Compilation: Minerals, *GRO.data*, V5. https://doi.org/10.25625/SGFTFN,

Draper, D.S., Johnston, A.D. (1992) Anhydrous PT phase relations of an Aleutian high-MgO basalt: an investigation of the role of olivine-liquid reaction in the generation of arc high-alumina basalts. *Contributions to Mineralogy and Petrology* 112, 501–519. https://doi.org/10.1007/bf00310781

Draper, D.S., duFrane, S.A., Shearer Jr., C.K., Dwarzski, R.E., Agee, C.B. (2006) High-pressure phase equilibria and element partitioning experiments on Apollo 15 green C picritic glass: Implications for the role of garnet in the deep lunar interior. *Geochimica et Cosmochimica Acta* 70, 2400–2416. http://doi.org/10.1016/j.gca.2006.01.027

Gaetani, G.A., Grove, T.L. (1998) The influence of water on melting of mantle peridotite. *Contributions to Mineralogy and Petrology* 131, 323–346. http://doi.org/10.1007/s004100050396

Gaetani, G.A., Grove, T.L. (2003) Experimental Constraints on Melt Generation in the Mantle Wedge. In: Eiler, J. (Ed.) *Inside the Subduction Factory*. Geophysical Monograph 138, American Geophysical Union, Washington, D.C., 107–134. http://doi.org/10.1029/138gm07

Grove, T.L., Holbig, E.S., Barr, J.A., Till, C.B., Krawczynski, M.J. (2013) Melts of garnet lherzolite: experiments, models and comparison to melts of pyroxenite and carbonated lherzolite. *Contributions to Mineralogy and Petrology* 166, 887–910. https://doi.org/10.1007/s00410-013-0899-9

Hirschmann, M.M., Kogiso, T., Baker, M.B., Stolper, E.M. (2003) Alkalic magmas generated by partial melting of garnet pyroxenite. *Geology* 31, 481–484. https://doi.org/10.1130/0091-7613(2003)031<0481:amgbpm>2.0.co;2

Holbig, E.S., Grove, T.L. (2008) Mantle melting beneath the Tibetan Plateau: Experimental constraints on ultrapotassic magmatism. *Journal of Geophysical Research: Solid Earth* 113, B04210. http://doi.org/10.1029/2007jb005149

Jackson, S. (2008) LAMTRACE data reduction software for LA-ICP-MS. In: Sylvester, P. (Ed.) *Laser Ablation ICP-MS in the Earth Sciences: Current Practices and Outstanding Issues*. Short Course Series v. 40, Mineralogical Association of Canada, Quebec, 305–307.

Jochum, K.P., Weis, U., Stoll, B., Kuzmin, D., Yang, Q., Raczek, I., Jacob, D.E., Stracke, A., Birbaum, K., Frick, D.A., Günther, D., Enzweiler, J. (2011) Determination of Reference Values for NIST SRM 610–617 Glasses Following ISO Guidelines. *Geostandards and Geoanalytical Research* 35, 397–429. https://doi.org/10.1111/j.1751-908x.2011.00120.x

Johnston, A.D. (1986) Anhydrous P-T phase relations of near-primary high-alumina basalt from the South Sandwich Islands. *Contributions to Mineralogy and Petrology* 92, 368–382. http://doi.org/10.1007/bf00572166

Keshav, S., Gudfinnsson, G.H., Sen, G., Fei, Y. (2004) High-pressure melting experiments on garnet clinopyroxenite and the alkalic to tholeiitic transition in ocean-island basalts. *Earth and Planetary Science Letters* 223, 365–379. https://doi.org/10.1016/j.epsl.2004.04.029

Kinzler, R.J. (1997) Melting of mantle peridotite at pressures approaching the spinel to garnet transition: Application to mid-ocean ridge basalt petrogenesis. *Journal of Geophysical Research: Solid Earth* 102, 853–874. https://doi.org/10.1029/96jb00988

Kogiso, T., Hirschmann, M.M. (2006) Partial melting experiments of bimineralic eclogite and the role of recycled mafic oceanic crust in the genesis of ocean island basalts. *Earth and Planetary Science Letters* 249, 188–199. http://doi.org/10.1016/j.epsl.2006.07.016

Kogiso, T., Hirschmann, M.M., Frost, D.J. (2003) High-pressure partial melting of garnet pyroxenite: possible mafic lithologies in the source of ocean island basalts. *Earth and Planetary Science Letters* 216, 603–617. http://doi.org/10.1016/s0012-821x(03)00538-7

Longhi, J. (1995) Liquidus equilibria of some primary lunar and terrestrial melts in the garnet stability field. *Geochimica et Cosmochimica Acta* 59, 2375–2386. http://doi.org/10.1016/0016-7037(95)00111-c

Longhi, J. (2002) Some phase equilibrium systematics of lherzolite melting: I. *Geochemistry, Geophysics, Geosystems* 3, 2001GC000204. http://doi.org/10.1029/2001gc000204

Mercer, C.N., Johnston, A.D. (2008) Experimental studies of the *P*–*T*–H_2O near-liquidus phase relations of basaltic andesite from North Sister Volcano, High Oregon Cascades: constraints on lower-crustal mineral assemblages. *Contributions to Mineralogy and Petrology* 155, 571–592. https://doi.org/10.1007/s00410-007-0259-8

Müntener, O., Kelemen, P.B., Grove, T.L. (2001) The role of H_2O during crystallization of primitive arc magmas under uppermost mantle conditions and genesis of igneous pyroxenites: an experimental study. *Contributions to Mineralogy and Petrology* 141, 643–658. https://doi.org/10.1007/s004100100266

Parman, S.W., Grove, T.L. (2004) Harzburgite melting with and without H_2O: Experimental data and predictive modeling. *Journal of Geophysical Research: Solid Earth* 109, B02201. http://doi.org/10.1029/2003jb002566

Pertermann, M., Hirschmann, M.M. (2003) Anhydrous Partial Melting Experiments on MORB-like Eclogite: Phase Relations, Phase Compositions and Mineral–Melt Partitioning of Major Elements at 2–3 GPa. *Journal of Petrology* 44, 2173–2201. https://doi.org/10.1093/petrology/egg074

Skjerlie, K.P., Johnston, A.D. (1996) Vapour-Absent Melting from 10 to 20 kbar of Crustal Rocks that Contain Multiple Hydrous Phases: Implications for Anatexis in the Deep to Very Deep Continental Crust and Active Continental Margins. *Journal of Petrology* 37, 661–691. https://doi.org/10.1093/petrology/37.3.661

Tenner, T.J., Hirschmann, M.M., Humayun, M. (2012) The effect of H_2O on partial melting of garnet peridotite at 3.5 GPa. *Geochemistry, Geophysics, Geosystems* 13, Q03016. http://doi.org/10.1029/2011gc003942

Ulmer, P., Kaegi, R., Müntener, O. (2018) Experimentally Derived Intermediate to Silica-rich Arc Magmas by Fractional and Equilibrium Crystallization at 1.0 GPa: an Evaluation of Phase Relationships, Compositions, Liquid Lines of Descent and Oxygen Fugacity. *Journal of Petrology* 59, 11–58. https://doi.org/10.1093/petrology/egy017

Vander Auwera, J., Longhi, J. (1994) Experimental study of a jotunite (hypersthene monzodiorite): constraints on the parent magma composition and crystallization conditions (*P*, *T*, f_{O2}) of the Bjerkreim-Sokndal layered intrusion (Norway). *Contributions to Mineralogy and Petrology* 118, 60–78. https://doi.org/10.1007/bf00310611

Walter, M.J. (1998) Melting of Garnet Peridotite and the Origin of Komatiite and Depleted Lithosphere. *Journal of Petrology* 39, 29–60. http://doi.org/10.1093/petroj/39.1.29

Wolf, M.B., Wyllie, P.J. (1994) Dehydration-melting of amphibolite at 10 kbar: the effects of temperature and time. *Contributions to Mineralogy and Petrology* 115, 369–383. https://doi.org/10.1007/bf00320972